In Situ and Time-Resolved SAXS Studies of Pd Nanoparticle Formation in a Template of Block Copolymer Microdomain Structures

Naoki Sakamoto,[†,§] Masafumi Harada,[†,⊥] and Takeji Hashimoto*[,†,‡,#]

Hashimoto Polymer Phasing Project, ERATO, Japan Science and Technology Corporation, and Department of Polymer Chemistry, Graduate School of Engineering, Kyoto University, Kyoto 615-8510, Japan

Received June 12, 2005; Revised Manuscript Received November 19, 2005

ABSTRACT: Time-resolved small-angle X-ray scattering (SAXS) measurements were performed to study in-situ formation of palladium (Pd) nanoparticles in block copolymer microdomains. The nanoparticles were reduced in a reaction medium containing a fixed composition of polyisoprene-*block*-poly(2-vinylpyridine) (PI-*b*-P2VP), palladium acetylacetonate, $Pd(acac)_2$, and benzyl alcohol as a solvent and a reducing agent. The polymer concentration is high enough so that it forms swollen ordered lamellae before reduction. The reduction was induced by a rapid temperature jump, and the polymer concentration was kept constant in a sealed sample cell. It was clearly elucidated that the formation of Pd nanoparticles occurred in the templates of the swollen lamellar microdomains. By fitting the theoretical scattered intensity for spherical particles to the observed SAXS profiles, we analyzed time evolution of mean radius, standard deviation of radius, and total volume of Pd nanoparticles in concentrated PI-*b*-P2VP solutions after T-jump. These results and the information obtained in our previous communication indicate that Pd(II) ions before reduction distribute equally well in both the PI and P2VP lamellae; after T-jump Pd nanoparticles form and grow only in the P2VP lamellae after an induction period, and the growth stops when the size reaches a steady value; the final size and total volume of Pd nanoparticles created depend on the reduction temperature. The formation of Pd nanoparticles in a P2VP homopolymer solution was also investigated by the same method as that employed for the block copolymer solution in order to compare the two results with and without the template and hence to explore roles of the template on the nanoparticle formation.

1. Introduction

In the recent decade metal nanoparticles having a diameter of the order of nanometers have been vigorously investigated. They are expected as innovative optoelectronic devices and catalyst because of their small size effect and extremely large specific surface area. However, the metal nanoparticles strongly tend to aggregate into large clusters; hence, in many cases they are stabilized by covering their surface with surfactants[1−3] or polymers.[4−20] Some researchers reported that the metal nanoparticles can be localized in a specific area of a specimen, i.e., a specific phase of microdomain structures by stabilizing metal nanoparticles with block copolymers.[8−20] The key points are that the block copolymers form the micorodomain structures and the one component of the block copolymers interacts with the metal more strongly than the other: the block copolymers act as both stabilizers for metal nanoparticles and templates controlling the distribution of them.

In our previous communication,[18] we reported the formation of the palladium (Pd) metal nanoparticles in the lamellar microdomain structure of polyisoprene-*block*-poly(2-vinylpyridine) (PI-*b*-P2VP) block copolymer. In that work, the concentrated solution of PI-*b*-P2VP in benzyl alcohol with palladium acetylacetonate, $Pd(acac)_2$, was annealed at 140 °C on a laboratory dish. By this annealing process, palladium ions, Pd(II), were reduced to Pd(0) by benzyl alcohol as a reduction agent, and benzyl alcohol acting also as a solvent was simultaneously evaporated; thus, PI-*b*-P2VP cast film with Pd metal nanoparticles could be obtained. The solutions before the annealing and the cast film containing Pd nanoparticles obtained after the annealing were investigated by small-angle X-ray scattering (SAXS) and transmission electron microscopy (TEM), respectively. The SAXS results indicated that the concentrated solutions before reduction of Pd(II) ions had a lamellar microdomaim structure where Pd(II) ions distributed equally well in the P2VP and PI lamellae. On the other hand, the TEM pictures for the cast film showed that Pd nanoparticles distributed only in P2VP lamellae. Figure 1 schematically presents a summary of the reduction process of Pd(II) ions and the reduction-induced formation of Pd nanoparticles in the solvent-cast process (i.e., the annealing process) employed in our previous work.

In this work, we focus on the kinetics of this reaction-induced self-assembling process of Pd nanoparticles in the organic templates to understand how the Pd nanoparticles are created and grow in the specific field of microphase (P2VP phase) of block copolymer templates. For this purpose we set up a well-defined experimental system which allows the reduction at a fixed polymer concentration and at a fixed temperature.

The observation of metal nanoparticle created by reduction of metal ions has been performed mainly by TEM,[1−20] wide-angle X-ray scattering (WAXS),[5,9] and SAXS.[9,11,18] The peak width analysis for the scattering from metal by WAXS allows us to obtain the size of metal crystals. However, we cannot detect the real size of metal nanoparticles if they consist of polycrystals. TEM analysis is not suitable for in situ observation of formation of metal nanoparticles. SAXS analysis may give

* To whom all correspondence should be addressed. E-mail: hashimoto.takeji@jaea.go.jp.
† Hashimoto Polymer Phasing Project, ERATO, JST.
‡ Kyoto University.
§ Present address: Analysis & Simulation Center, Asahi Kasei Corporation, Shizuoka 416-8501, Japan.
⊥ Present address: Department of Textile and Apparel Science, Faculty of Human Life and Environment, Nara Women's University, Nara 630-8506, Japan.
Present address: Advanced Science Research Center, Japan Atomic Energy Agency, Tokai-mura, Ibaraki 319-1195, Japan.

10.1021/ma051233j CCC: $33.50
Published on Web 12/31/2005

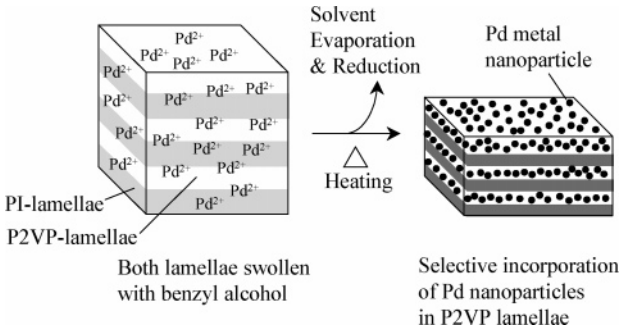

Figure 1. Schematic representaion on summary of our previous work.[18] PI-*b*-P2VP concentrated solution in benzyl alcohol with molecularly dissolved $Pd(acac)_2$ had alternating lamellar microdomains (swollen with benzyl alcohol); $Pd(acac)_2$ and benzyl alcohol are uniformly distributed in the solution because of strong attractions of $Pd(acac)_2$ with benzyl alcohol rathar than PI and P2VP block chains. Heating the solution at 140 °C resulted in reduction of Pd(II) ions to Pd(0) atoms, and Pd nanoparticles were selectively incorporated in P2VP phase, owing to their stronger attractive interactions with P2VP block chains rather than PI block chains. The heating simultaneously evaporated benzyl alcohol, yielding polymer films containing Pd nanoparticles with a unique spatial distribution.

Table 1. Characterization of Polymers Used in This Work

	M_n	f_{P2VP}	M_w/M_n
PI-*b*-P2VP	3.1×10^4	0.4	1.04
P2VP	3.8×10^4	1.0	<1.1

information for both metal nanoparticles and microdomain structures. Cohen and his coworkers[9,11] presented the SAXS profiles from the microphase-separated organometallic-*block*-organic block copolymer before and after reduction of metal complex. The SAXS profile before reduction showed the scattering only from the microdomain structure, while that after reduction showed the scattering from both the microdomain structure and metal nanoparticles. Moreover, the scattering analysis gave information on the size of metal nanoparticles.

However, those SAXS measurements were performed only before reduction and after completion of reduction process. Hence, kinetics of nanoparticle formation in the templates have hardly been investigated so far, and mechanisms and processes of the hybrid formation remain essentially unclarified. We thus performed time-resolved SAXS measurements during the reduction reaction process of concentrated polymer solutions containing $Pd(acac)_2$ at a fixed polymer concentration, induced by a temperature jump (T-jump) to 80 and 100 °C. The time-resolved SAXS is well-known as a powerful tool for in-situ observation of nanostructure formation process.[21,22] We hope we could make some contributions to illuminate basic physics underlying this problem.

2. Experimental Methods

2.1. Sample Preparation. PI-*b*-P2VP diblock copolymer and P2VP homopolymer used in this work were synthesized as detailed elsewhere.[23,24] The number-average molecular weight, M_n, the volume fraction, f_{P2VP}, of P2VP in block copolymer, and the heterogeneity index, M_w/M_n, of these polymers are listed in Table 1. The concentrated solution of block copolymer or homopolymer with $Pd(acac)_2$ was prepared as follows: (1) prescribed amounts of polymer, benzyl alcohol, and $Pd(acac)_2$ were dissolved into an excess amount of chroloform to obtain a dilute homogeneous solution; (2) chloroform was completely evaporated at room temperature (RT). The solution thus obtained was a clear brown solution without any reduction of Pd(II) ions. The composition of the solution is listed in Table 2.

2.2. SAXS Measurements. The time-resolved SAXS measurements were performed to observe the formation of Pd nanoparticles

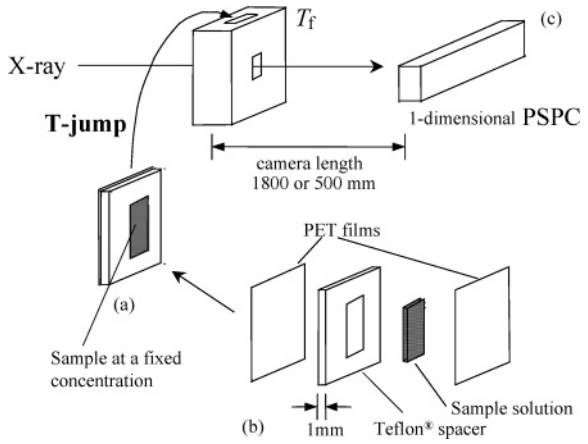

Figure 2. Schematic illustration for the T-jump, time-resolved SAXS experimental method for a fixed and high concentration solution of P2VP-*b*-PI block copolymer or P2VP homopolymer with benzyl alcohol as a solvent and reducing agent for $Pd(acac)_2$. The time required for reaching the target temperature T_f is within 1 min.

Table 2. Summary of the T-Jump Experiments

weight composition in sample					
PI-*b*-P2VP	P2VP	$Pd(acac)_2$	benzyl alcohol	T_f (°C)	results
0.29	0	0.12	0.59	80	Figures 3, 4
0.29	0	0.12	0.59	100	Figure 5
0	0.29	0.12	0.59	80	Figure 6

in the concentrated polymer solution. Figure 2 presents a schematic illustration of time-resolved SAXS measurements after T-jump of the solution prepared at RT to temperatures, T_f, where the reduction of Pd(II) ions takes place in the solution with the fixed composition of the components. The T-jump process was done as follows: (1) the specimen was placed in the sample cell shown in part a of Figure 2, where the solution was placed in the Teflon spacer with the both sides of the window sealed by poly(ethylene terephthalate) (PET) films of 14 μm thickness as shown in part b; (2) the sample cell was put manually into the heater block which was set on the optical path of incident X-ray beam and regulated at T_f as shown in part c; (3) time-resolved SAXS measurements were started and time t was set zero at the time when the specimen was put into the heater block at T_f. The temperature in the sample reaches the T_f within 1 min after T-jump. Here it should be noted that in the previous work the reduction of Pd(II) ions and the evaporation of extra amounts of benzyl alcohol were done by a single annealing process at 140 °C. This process has an advantage to obtain a film in which Pd nanoparticles are incorporated selectively in P2VP lamellae by a single step process. However, this single step process is complicated for analyzing the self-assembling mechanism. To simplify the system, the samples were annealed in a sealed cell at a constant composition, as shown in Figure 2, in this study. Thus, we could avoid the evaporation of the solvent and observe the change involved only by the reduction of Pd(II) ions. The composition of the polymer solution with $Pd(acac)_2$ and T_f are listed in Table 2.

The scattered intensity was measured with the SAXS apparatus[21,25] which consists of an 18 kW rotating-anode X-ray generator (Bruker AXS K.K., Ibaraki, Japan), a graphite crystal for incident-beam monochromatization, and a one-dimensional position-sensitive proportional counter (PSPC). The SAXS profiles were obtained with a camera length of 1800 or 500 mm. The profiles obtained were corrected for absorption and air scattering as described elsewhere.[25]

3. Experimental Results

Figure 3 gives the time evolution of the SAXS profiles of the PI-*b*-P2VP solution after T-jump to 80 °C, obtained with the camera length of 500 mm. The SAXS intensity is plotted

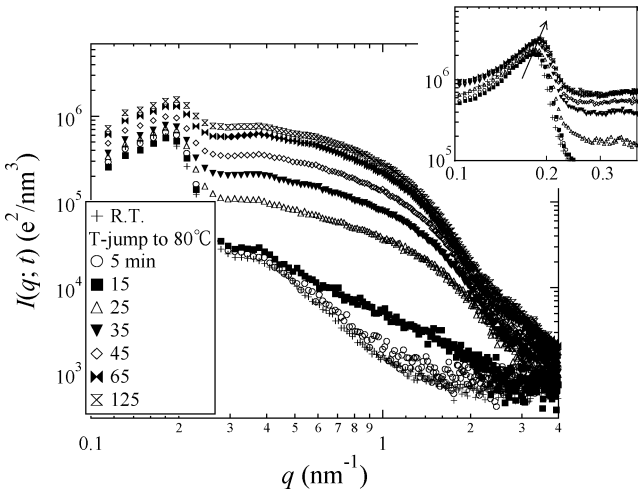

Figure 3. Time evolution of SAXS profiles of the PI-*b*-P2VP solution after T-jump to 80 °C. The data in the large graph were obtained with the camera length (distance between the sample and the detector) of 500 mm. The inset shows the profiles focused on the first-order peak obtained with the camera length of 1800 mm.

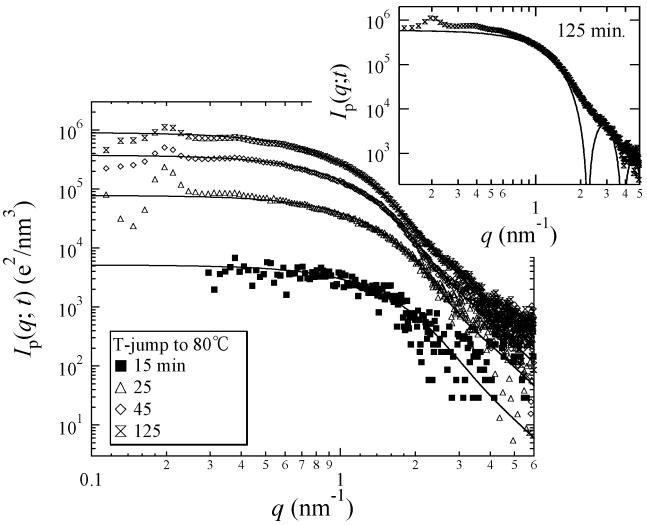

Figure 4. Time evolution of SAXS intensity from Pd nanoparticles, calculated on the basis of eq 2 after T-jump of the PI-*b*-P2VP solution to 80 °C. Solid lines show the predicted curves best-fitted with the experimental curves, $I_p(q;t)$, by using eq 3. The inset presents $I_p(q;t =$ 125 min) as a typical profile after formation of Pd nanoparticles. The solid line in the inset presents the calculated curve from the isolated spheres with a monodisperse sphere size, $R_0 = 1.9$ nm and $\sigma_R = 0$ nm.

as a function of the scattering vector q. The quantity q is defined by

$$q = (4\pi/\lambda)\sin(\theta/2) \tag{1}$$

where λ and θ are the wavelength and scattering angle in the medium, respectively. In Figure 3 the SAXS profile at RT is also plotted as a reference for the solution without reduction. The SAXS profile at RT before reduction of Pd(II) ions shows the scattering maximum at $q = 0.18$ and 0.36 nm^{-1}, indicating that the PI-*b*-P2VP solution has lamellar structure with lamellar spacing of 35 nm. The inset shows the profiles focused on the first-order peak obtained with the camera length of 1800 mm in order to observe the time changes in the lamellar microdomain structure. In Figure 3, the following observations are worth noting: (1) the SAXS profiles for the solution annealed for less than 5 min (open circles) are essentially same as the initial profile, reflecting an induction period for the Pd particle formation as will be clarified later; (2) the SAXS intensity at $q > 0.25$ nm^{-1} increases with time after 15 min; (3) the scattered intensity almost reaches a steady value at 65 min; (4) the first-order scattering maximum, q_m, slightly shifts to larger q with time (see the inset); (5) the second-order peak from lamellae still exists even after the reduction; (6) the excess scattering emerging after T-jump tends to show a broad peak or shoulder at the large q-limit in Figure 3 ($q > 2$ nm^{-1}). This trend is also seen in Figure 4 as will be shown later. The increased scattered intensities at $q > 0.25$ nm^{-1} after 15 min should originate from the Pd nanoparticle created by reduction at the annealing temperature. The broad peak or shoulder at the large q limit in Figures 3 and 4 arises from a form factor of Pd nanoparticles. The SAXS profile, $I(q;t)$, in Figure 3 is composed of $I_d(q;t)$ from the microdomain structure formed in PI-*b*-P2VP solution and $I_p(q;t)$ from Pd nanoparticles formed after reduction of Pd(II) ions into atoms and their aggregation into nanoparticles.[27]

To analyze the formation of Pd nanoparticles, we tried to separate $I_p(q;t)$ from $I(q;t)$. Although $I_d(q;t)$ changes with time as shown in the inset of Figure 3, the contribution of $I_d(q;t)$ to $I(q;t)$ at $q > 0.25$ nm^{-1} is relatively small; hence, we assume that $I_p(q;t)$ is expressed by

$$I_p(q;t) = I(q;t) - I_0(q),\ I_d(q;t) \cong I_0(q) \tag{2}$$

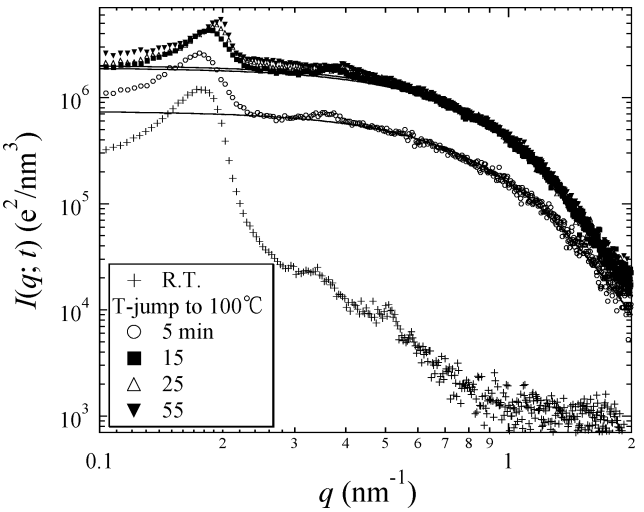

Figure 5. Time evolution of SAXS profiles after T-jump of the PI-*b*-P2VP solution to 100 °C. Solid lines show the predicted curves best-fitted with the experimental curves, $I_p(q;t)$, by using eq 3.

where $I_0(q)$ is the initial SAXS profile at RT. $I_p(q;t)$ calculated by eq 2 is plotted as a function of q in Figure 4. The curves shown by solid lines will be discussed later in section 4. The inset of Figure 4 presents $I_p(q;t = 125$ min) in order to show clearly the typical profile after formation of Pd nanoparticles. The inset reveals that the $I_p(q;t = 125$ min) has a broad peak at $q = 3$ nm^{-1}, arising from a form factor of Pd nanoparticles. The broad peak can be observed in the other $I_p(q;t)$ also, except for that at 15 min. The form factor peak may become clear when it is compared with that from isolated spheres with a monodisperse sphere size, as shown by the solid line in the inset of Figure 4.

Figure 5 presents the time evolution of the SAXS profiles of the PI-*b*-P2VP solution after T-jump to 100 °C. The SAXS intensity is plotted as a function of q; the SAXS intensity increases with time and reaches nearly steady intensity at 15 min after the T-jump. The value of q_m slightly shifts to larger q values with time as found in Figure 3. The curves shown by solid lines will be discussed later in section 4.

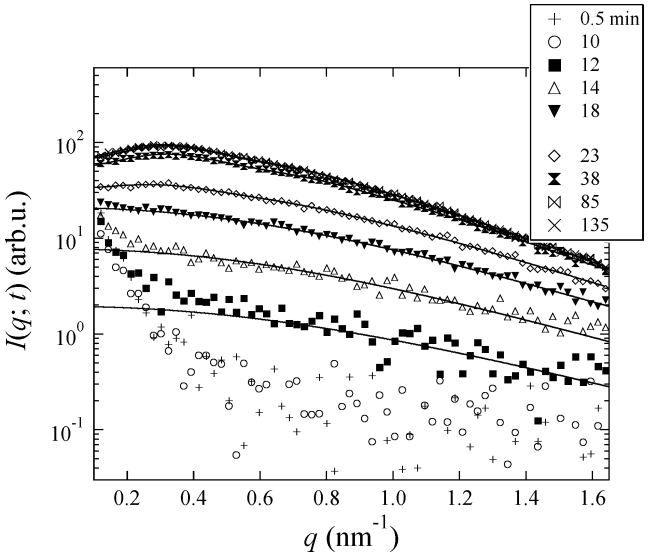

Figure 6. Time evolution of SAXS profiles after T-jump of the P2VP solution to 80 °C. Solid lines show the predicted curves best-fitted with the experimental curves, $I(q;t)$, by using eq 6.

Figure 6 shows the time evolution of the SAXS profiles of the P2VP homopolymer solution after T-jump to 80 °C. The SAXS intensity stays identical to that in the initial state for 10 min, begins to increase at 12 min, and reaches almost steady intensity at 38 or 85 min. Here it should be noted that the SAXS profiles after 23 min show the maximum at the q near 0.3 nm^{-1}, although the P2VP solution should not have a microdomain structure. We shall go into detail discussion about the scattering maximum in section 4.

4. Analysis and Discussion

4.1. Time Evolution of Pd Nanoparticles in a Templete of Swollen Microdomain Structures. As shown in section 3, the SAXS profile, $I(q;t)$, in Figures 3 and 5 is composed of the scattering from the microdomain structure and that from Pd nanoparticles. If the Pd particles is spherical and the distribution of them has no correlation, the latter scattering, $I_p(q;t)$, is approximately expressed by[26]

$$I_{p,theory}(q;t) = CN\int_0^\infty P(R)\left[\frac{4\pi R^3}{3}\Phi(qR)\right]^2 dR \qquad (3a)$$

$$\Phi(qR) = \frac{3}{(qR)^3}[\sin(qR) - (qR)\cos(qR)] \qquad (3b)$$

where R is a radius of spherical particles, N is total number of particles, $P(R)$ is a normalized distribution function describing a number of particles having radius R, and C is a constant independent of q and R. In eq 3 we assume that $P(R)$ has the Schultz−Zimm distristribution defined by

$$P(R) = \frac{M^M}{\Gamma(M)R_0^M}R^{M-1}\exp\left(-\frac{M}{R_0}R\right), \quad \int_0^\infty P(R)\,dR = 1 \quad (4)$$

where M is a shape factor of the distribution, R_0 is a number-average of R, and $\Gamma(x)$ is the gamma function. If the value of M in eq 4 is sufficiently large, the Schultz−Zimm distribution can be approximated by the Gauss distribution, and if $M = 1$, it is equal to the exponential. We note that R_0, N, and $P(R)$ in eqs 3 and 4 are generally a function of t after T-jump.

In Figures 4 and 5, the solid lines show the best-fitted curves, $I_{p,theory}(q;t)$, obtained by eqs 3 and 4 with $I_p(q;t)$ after T-jump to 80 and 100 °C, respectively, though $I_p(q;t)$ after T-jump to 100 °C is not presented. Figures 4 and 5 reveal that $I_p(q;t)$ can be well described by eqs 3 and 4. The $P(R)$'s thus obtained by fitting for the SAXS profiles after T-jump to 80 °C are plotted in Figure 7. The function $P(R)$ shifts to larger R with time. The details about the time dependence of R_0, reduced standard deviation, σ_R/R_0, and total volume of Pd nanoparticles, V_p, calculated by $P(R)$ and N obtained by the fitting are discussed later in Figures 9, 10, and 11, respectively. For the profile at 25 min after T-jump to 80 °C, we performed the fitting based on the assumption that $P(R)$ is given by the zeroth-order logarithmic distribution (ZOLD)[28] described by eq 5 below as well as the Schultz−Zimm distribution.

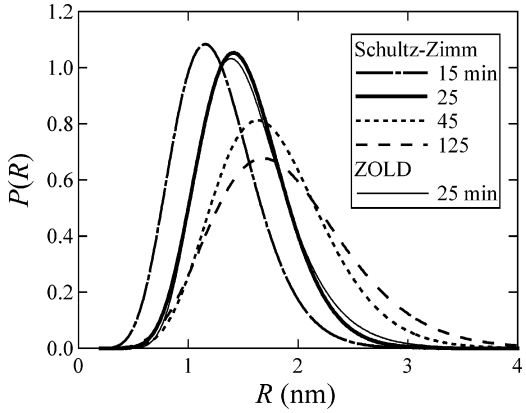

Figure 7. Time changes in the distribution of R, $P(R)$, after T-jump of the PI-*b*-P2VP solution to 80 °C, calculated by fitting eq 3 to the experimental curves. The $P(R)$'s at 25 min were obtained with the zeroth-order logarithmic distribution (ZOLD) described by eq 5 as well as the Schultz−Zimm distribution described by eq 4.

$$P(R) = \frac{1}{\sqrt{2\pi}\Delta R_M \exp(\Delta^2/2)}\exp\left[-\frac{(\ln R - \ln R_M)^2}{2\Delta^2}\right] \quad (5)$$

In eq 5 R_M and Δ are closely related to R_0 and standard deviation, σ_R, respectively: if Δ is sufficiently small, R_M and Δ are equal to R_0 and σ_R, respectively. Figure 7 shows that the $P(R)$'s for 25 min after T-jump expressed by ZOLD and Schultz−Zimm distribution are almost the same, indicating that both distribution functions can describe equally well the real distribution of R for this particular case.

In eq 3, we assume that the Pd nanoparticles have no spatial correlation with each other; i.e., the scattering from the Pd nanoparticles can be expressed by a sum of the scattering from isolated spheres. However, because the Pd nanoparticles exist only in the P2VP phase of microdomain structure, the Pd nanoparticles should have the correlation corresponding to the long-range order of mirodomain structure. Nevertheless, we confirmed that the scattering from the Pd nanoparticles at $q >$ 0.6 nm^{-1} can be approximately expressed by eq 3 in our case, simply because an oscillation of the lattice factor with q due to the long-range order is damped to a constant level at $q > 0.6$ nm^{-1}. The general formula of the scattering function from microdomain templates with nanoparticles and the precise analysis for the scattering obtained in this experiment will be presented elsewhere.[27] In Figure 4 it should be noted that the small scattering maximum can be observed at 0.38 nm^{-1} on the $I_p(q;t)$'s at 25, 45, and 125 min, which is nearly equal to the position of the second-order scattering maximum from the microdomain template. It originates from the correlation between Pd nanoparticles in a lamellar template and those in the other, i.e., the interlamellar correlation of Pd nanoparticles and hence

a maximum in the lattice factor for the spatial distribution of the microdomains.

4.2. Time Evolution of Pd Nanoparticles in P2VP Homopolymer Solutions. In Figure 6, the SAXS profiles after 23 min show the scattering maximum at the q value nearly equal to 0.3 nm^{-1}, although the P2VP solution do not have the microdomain structure. It means that some local liquidlike orders are developed for a spatial distribution of Pd nanoparticls. We assume that the liquidlike order of the nanoparticles arises from entropic repulsions of swollen P2VP chains, which are adsorbed by the nanoparticles, in the solution of free P2VP chains. These adsorbed chains may have loops and/or tail configurations as proposed by our earlier works[29−31] and are defined hereafter as coronal chains ("corona"). The schematic illustration of this model is shown in part a of Figure 8, where R is the radius of Pd nanoparticle, l_{corona} is the layer thickness of adsorbed chains of P2VP (corona), a is R plus l_{corona}, and d is the interparticle distance. In this model, the Pd particles plus the adsorbed P2VP chains, represented by the "spheres" shown by the broken lines in Figure 8, are assumed to be "hard spheres" in the matrix solution of free P2VP chains: these "spheres" are assumed not to penetrate each other as schematically shown by the pair distribution function of the hard sphere, $P_{pair}(r)$, in part c. On the other hand, the scattering mainly arises from the Pd core as shown by the electron density distribution, $\rho(r)$, in part b. Kinning et al.[32] and Cohen et al.[9,11] applied a similar model respectively to spherical microdomain structures of bulk block copolymers and to Pt and Pd nanoparticles in the block copolymers, both having liquidlike order. The theoretical scattered intensity, $I_{HS}(q)$, for this hard-sphere model is given by[32,33]

$$I_{HS}(q) = CNS(q,a,\eta)\int_0^\infty P(R)\left[\frac{4\pi R^3}{3}\Phi(qR)\right]^2 dR \quad (6a)$$

$$S(q,a,\eta) = \frac{1}{1 + 24\eta[G(A)/A]} \quad (6b)$$

$$G(A) = \frac{\alpha}{A^2}(\sin A - A\cos A) + \frac{\beta}{A^3}[2A\sin A + (2 - A^2)\cos A - 2] + \frac{\gamma}{A^5}(-A^4\cos A + 4[(3A^2 - 6)\cos A + (A^3 - 6A)\sin A + 6]) \quad (6c)$$

$$\alpha = (1 + 2\eta)^2/(1 - \eta)^4 \quad (6d)$$

$$\beta = -6\eta(1 + \eta/2)^2/(1 - \eta)^4 \quad (6e)$$

$$\gamma = \frac{1}{2}\eta(1 + 2\eta)^2/(1 - \eta)^4 \quad (6f)$$

$$A = 2qa \quad (6g)$$

Here η is volume fraction of hard spheres.

In Figure 6, the calculated scattered intensity based on eq 6 with Schultz−Zimm distribution of R ($P(R)$ in eq 4) is shown by solid lines. The results reveal that the scattering intensity distributions including the scattering maximum can be well described by the hard sphere model: the maximum originates from the excluded-volume effect. The time evolution of the number-average radius of the Pd particles, R_0, evaluated by using eq 6 will be shown later in Figure 9. The values of η and a after T-jump change from 0 to 0.06 and from 7.6 to 8.0 nm, respectively. Here it should be noted that eq 6 is derived for the system in which a has a monodispersity. If the dispersity

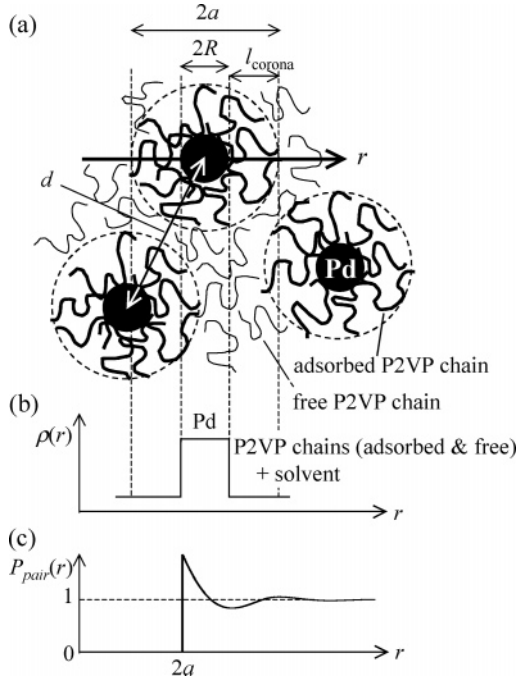

Figure 8. (a) Schematic illustration for the hard-sphere model with the core−shell structure having R, l_{corona}, a, and d. The P2VP chains adsorbed to Pd nanoparticles and the free ones are shown by bold and thin lines, respectively. Part (b) indicates the electron density profile across the core−shell structure along the solid line in (a). The Pd particles including adsorbed chains of P2VP, shown by the broken circles, are considered as hard spheres having the pair distribution function, $P_{pair}(r)$, as shown in (c).

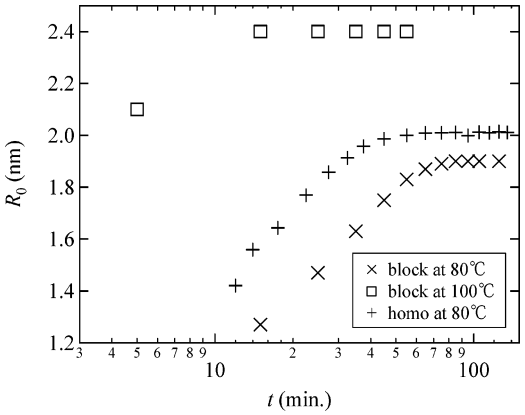

Figure 9. Time changes in the average radius, R_0, of the Pd nanoparticles obtained by fitting the theoretical curves obtained by eq 3 or 6 to the experimental curves.

of a is quite large, eq 6 cannot be applied. In our case, $a \equiv R + l_{corona}$ as shown in Figure 8. The value a estimated by best-fitting $I_{HS}(q)$ with the experimental scattering profile changes from 7.6 to 8.0 nm with time, while the mean radius, R_0, of Pd nanoparticles changes from 1.4 to 2.0 nm with time as will be shown later in Figure 9. Hence, the l_{corona} should be equal to about 6 nm in the whole time region after T-jump. If the l_{corona} can be assumed to be constant and equal to 6 nm, the reduced standard deviation of a, expressed by $\sigma_a/a_0 = \sigma_a/(R_0 + l_{corona})$ where σ_a and a_0 are the standard deviation of a and mean value of a, respectively, can be estimated by using the value R_0 and σ_R/R_0, which will be shown later in Figures 9 and 10, respectively. The values of σ_a/a_0 thus obtained are less than 0.1, which are sufficiently small so that eq 6 may be applied to the analysis of the SAXS profile after T-jump of P2VP solution to 80 °C.

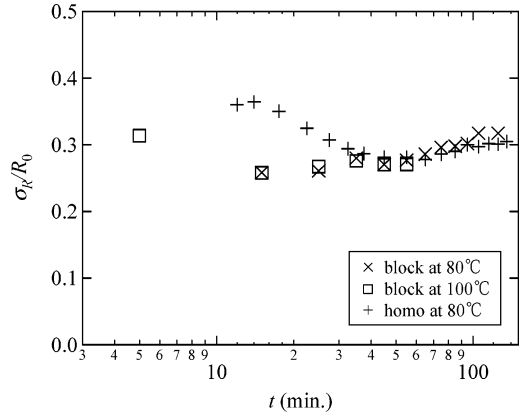

Figure 10. Time changes in the σ_R/R_0 of the Pd nanoparticles, evaluated by fitting the theoretical curves obtained eq 3 or 6 to the experimental curves. The σ_R/R_0 is expressed by eq 7 by using the value of M in the Schultz−Zimm distristribution (eq 4).

4.3. Comparison of Pd Nanoparticle Formation with and without the Microdomain Template. Figure 9 gives the time changes in the R_0 evaluated by fitting the predicted scattering curves based on eq 3 or 6 to the experimental curves. In Figure 9, the R_0 begins to increase after an induction time and reaches a steady value. The final size of Pd nanoparticles as well as the growth rate depends on the temperature: the size and the growth rate of Pd nanoparticles are larger when the reduction takes place at a higher temperature. The Pd particles formed in the P2VP homopolymer solution at 80 °C are slightly larger and grow faster than those in the P2VP-*b*-PI block copolymer solution at 80 °C.

Figure 10 gives the time-changes in the σ_R/R_0 of Pd nanoparticles obtained by fitting the predicted scattering curves based on eq 3 or 6 to the experimental curves. The value of σ_R is expressed as follows in the case of the Schultz−Zimm distribution by using the value, M, in eq 4.

$$\sigma_R = \langle (R - R_0)^2 \rangle^{1/2} \tag{7a}$$

$$\sigma_R/R_0 = M^{-0.5} \tag{7b}$$

In Figure 10, it should be mentioned that the σ_R/R_0 for the PI-*b*-P2VP solution as well as for the P2VP solution hardly depends on reduction temperature and time, implying that size distribution of Pd nanoparticles approximately changes self-similarly with time.

Figure 11 shows the total volume, V_p, of Pd particles in the P2VP-*b*-PI solution, plotted as a function of time. The V_p is expressed by

$$V_p = N \int_0^\infty P(R) \frac{4}{3} \pi R^3 \, dR \tag{8}$$

The $t_{1/2}$'s defined as the time when V_p reaches the half of the final value, $V_{p\infty}$, are also shown here. In Figure 11 it should be noted that the V_p's at 80 and 100 °C sigmoidally increase with time and saturate at the different values: the saturated value of V_p at 100 °C is larger than that at 80 °C. It indicates that the total amount of Pd metals produced by reaction depends on reduction temperature: Pd metals are created more at 100 °C than at 80 °C, although the initial amount of Pd(II) ions is the same for the two cases. The $t_{1/2}$ at a given temperature (80 °C) in the homopolymer solution is about the same as that in the block copolymer solution.

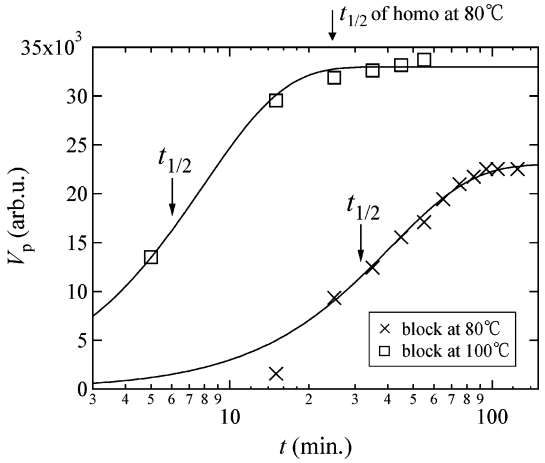

Figure 11. Time changes in the value V_p calculated by eq 8: V_p is the total volume of Pd particles after T-jump of the block copolymer solution to 80 (×) and 100 °C (□). The N and $P(R)$ in eq 8 are obtained by fitting eq 3 to the SAXS profiles, $I_p(q;t)$. $I_p(q;t)$ is calculated by eq 2. The $t_{1/2}$'s defined in the text are also marked here for the P2VP homopolymer solution ($t_{1/2}$ of homo) as well as for the block copolymer solutions.

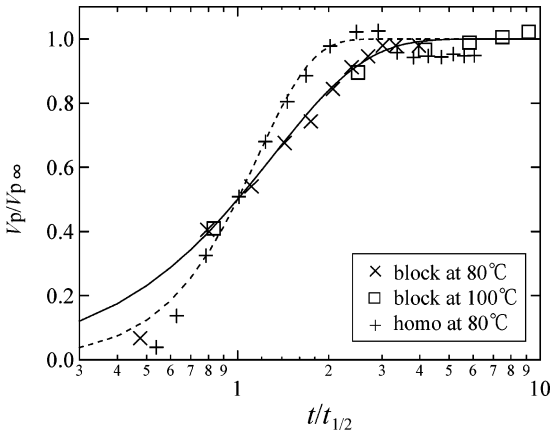

Figure 12. Reduced total volume of Pd particles, $V_p/V_{p\infty}$, plotted as a function of reduced time, $t/t_{1/2}$, after T-jump of the PI-*b*-P2VP block copolymer solution to 80 (×) and 100 °C (□) and the P2VP homopolymer solution to 80 °C (+). Solid and broken lines show the predicted curves best-fitted by using eq 10 with the experimental curves of the PI-*b*-P2VP and the P2VP solutions, respectively.

Figure 12 presents the reduced total volume of the Pd particles, $V_p/V_{p\infty}$, plotted as a function of the reduced time, $t/t_{1/2}$. The plot of $V_p/V_{p\infty}$ vs $t/t_{1/2}$ is useful to analyze the nucleation and growth (NG) process because this plot depends mainly on the NG mechanism as will be detailed below. Avrami analysis is one of the popular method to analyze the NG process of crystals (Pd particles in our case), where the time evolution of crystallinity (e.g., volume fraction of crystals), X, is assumed to be expressed by[34]

$$X = 1 - \exp(-Kt^n) \tag{9}$$

The parameter K is a constant which depends on density of nuclei and growth rate of a crystal, and n is Avrami number which is closely related to the NG mechanism. If we apply Avrami method to our result, and if the X is replaced by the $V_p/V_{p\infty}$, then eq 9 can be rewritten by

$$V_p/V_{p\infty} = 1 - \exp[-(t/t_{1/2})^n \ln 2] \tag{10}$$

Equation 10 means that the difference in the plot of $V_p/V_{p\infty}$ vs $t/t_{1/2}$ arises from the difference of the "apparent" Avrami number

n, i.e., the NG mechanism. In our method, the term NG refers to NG of Pd atoms formed after reduction into the nanoparticles that can be detected by the SAXS method. Figure 12 shows that the curves of the PI-*b*-P2VP solution obtained after T-jump to 80 and 100 °C are completely the same; however, that of the P2VP solution is different, indicating that the NG mechanism of the Pd nanoparticles in the PI-*b*-P2VP solution at 80 and 100 °C is identical but that in the P2VP solution is different. In Figure 12, the predicted curves are obtained with $n = 1.4$ and 2.4 in eq 10 for the PI-*b*-P2VP and the P2VP solutions, respectively, although it is difficult to give a physical interpretation for the difference in the number *n*.

Here it should be noted that Pd(II) ions before reduction exists uniformly in the P2VP and PI lamellae in the concentrated block copolymer solution, but Pd nanoparticles after reduction are selectively incorporated in a P2VP lamellae as clarified previously[18] and demonstrated in Figure 1. From the previous results and the analyses discussed above, Pd nanoparticles are considered to be created in the microdomain structure after T-jump as follows: (1) Pd(II) ions existing uniformly in space are reduced into Pd(0) atoms; (2) the reduced Pd atoms diffuse and coalesce into nanoparticles which are localized in a P2VP phase because Pd particles may have a larger affinity to P2VP chains than to PI chains and the solvent; (3) Pd nanoparticles, which exceed the size of critical nuclei, grow by attracting and absorbing newly reduced Pd atoms or by diffusion−coalescence of nanoparticles; (4) the particles grown into a large size reduce their mobility and increase the interaction sites with P2VP. Hence they are trapped by P2VP chains and cannot grow into a larger size anymore via the diffusion−coalescence process, though they may still grow by absorbing Pd(0) atoms. The final size and total volume of Pd nanoparticles created depend on the reduction temperature. However, the apparent Avrami number obtained in Figure 12 is independent of a temperature for PI-*b*-P2VP, meaning that the NG mechanism does not change with a reduction temperature if a templates of a microdomain structure is identical. In the process (1) shown above, Pd(II) ions in solution are considered to be reduced in both the PI and P2VP phases because Pd(II) ions can be reduced without polymer at 80 °C. However, we cannot determine whether the reduction occurs uniformly in space or more easily in the P2VP or PI phase from this study. It should be reserved for future investigations.

Those differences in the NG mechanism and the growth rate as described above between the P2VP homopolymer system and the block copolymer system may be interpreted on the basis of the differences in the cost of elastic free energy of polymer chains caused by the incorporation of the Pd particles in the system. In the case of homopolymer solution, P2VP chains exists in free space, though they are subjected to entanglements. When the Pd particles are incorporated in the space, we should think of the cost of elastic free energy due to the loss of conformational entropy of the entangled chains in the matrix and the chains adsorbed by growing Pd particles. However, the cost can be effectively relaxed by a spatial rearrangement of the chains via disentanglement processes. On the other hand, P2VP block chains in lamellar microdomains are confined in the lamellar space with their one ends (chemical junctions with PI block chains) at the interface of P2VP and PI phases. Thus, the cost discussed above cannot be effectively relaxed but rather tend to be stored in the lamellar system as a whole via changes in the thickness of lamellae and in an average interfacial area per a single block chain as will be described below. The difference in the relaxation of chains in the two systems may affect the diffusion−coalescence of Pd particles and hence results in the difference in the NG mechanism and its growth rate. Thermal concentration fluctuations and fluctuations between entanglements in P2VP homopolymer solutions may cause the enlarged size distribution, especially in the early stage of the reduction process, as observed in Figure 10.

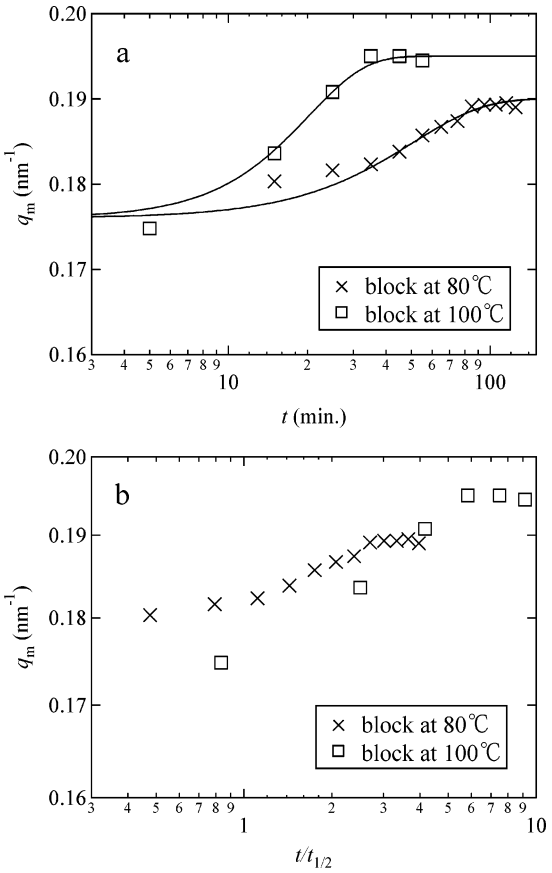

Figure 13. (a) Time changes in the value of q_m reflecting the time evolution of the microdomain structure accompanied by formation of the nanoparticles after T-jump of the block copolymer solution to 80 (×) and 100 °C (□). The solid lines are visual guides. (b) log q_m vs log $t/t_{1/2}$ where $t_{1/2}$ was estimated from Figure 11.

4.4. Time Evolution of the Microdomain Structure Induced by Nanoparticle Formation. In Figure 13a, the q_m's obtained from Figures 3 and 5 are plotted as a function of time after T-jump of the PI-*b*-P2VP solution to 80 and 100 °C. We note that the magnitude of scattering vector before the reduction and that immediately after the reduction at 80 and 100 °C are the same. The increase of q_m's implies that the domain spacing decrease with time, although Pd particles are created in P2VP lamellae. We may offer the following possible conjecture. Pd nanoparticles selectively incorporated into P2VP lamellae may increase an average distance between the chemical junctions of P2VP and PI blocks at the interface. This effect tends to decreases thickness of both PI and P2VP lamellae (effect i), but an increased volume of P2VP lamellae due to the Pd particles tends to increase thickness of the P2VP lamellae (effect ii). We anticipate effect i outweights effect ii, giving rise to the net decrease of the lamellar spacing and hence increase of q_m with increasing amount of Pd nanoparticles. Because the total volume of Pd particles at 100 °C is more than that at 80 °C as shown in Figure 11, the change in the value of q_m at 100 °C is larger than that at 80 °C.

We should note the growth rates of the particles at 80 and 100 °C are different (as seen in the difference in $t_{1/2}$ in Figure

11), so that the change in the lamellar spacing, $2\pi/q_m$, with time is also different at these temperatures. Thus, the q_m's were replotted as a function of the reduced time $t/t_{1/2}$ in Figure 13b. The results elucidate that the trends at these two temperatures become closer to each other on the reduced time scale, revealing that the change in the lamellar spacing with time tends to be affected by the growth rate of the Pd particles in P2VP lamellae.

4.5. Comparison with Earlier SAXS Results. Cohen and co-workers[9,11] explored the microdomain structures for the organometallic-*block*-organic diblock copolymer, Pd(Cp^N)PA-*block*-MTD or Pt(Cp^N)Me_3-*block*-MTD, where Pd, Pt, Cp^N, PA, and MTD are palladium, platinum, *endo*-2-(cyclopentadienylmethyl)norborn-5-ene, η^3-1-phenylallyl, and methyltetracyclododecene, respectively. They also observed effects of the reduction reaction on the microdomain structures and on metal nanoparticle formation by SAXS. Instead of the concentrated block copolymer solution, however, they used the solution-cast films; instead of the time-resolved studies, they conducted the SAXS studies only before and after the reduction. The Pd and Pt in the block copolymers were reduced with hydrogen at 100 °C far below the T_g (~210 °C) of polyMTD (host) polymer matrix. The block copolymer containing Pt was exposed by the UV light before the reduction process described above. Thus, the reaction condition and the reduction environment employed by them are quite different from ours, which makes proper comparisons of the two results very difficult. Nevertheless, we tried to address our few remarks below.

The SAXS profiles for Pt(Cp^N)Me_3-*block*-MTD before reduction exhibited the first-order peak at $q_{m1} \cong 0.17$ nm^{-1} and the second-order peak at $q_{m2} \cong 0.29$ nm^{-1}, relevant to the hexagonal cylinders in the host hard matrix of polyMTD. After the reduction the first-order peak slightly shifts to 0.18 nm^{-1}; the second-order peak at q_{m2} completely disappeared and was reflected by the large excess scattering with a very broad peak centered at $q_m \cong 0.31$ nm^{-1}. They claimed that the cylindrical feature was maintained even after reduction and that the broad high-intensity peak is due to the "cluster−cluster spacings" of Pt particles primarily formed in the cylinder.

We can find the difference between their and our results as follows. The second-order scattering maximum for the specimens after reduction of metal ions could be observed in our case (see Figures 3 and 5), while it could not in their case. The scattering theory[27] predicts that the higher order maxima should be observed as long as the hexagonal lattice is maintained after loading the Pt particles selectively in the cylindrical microdomains, though the higher order peak becomes not only more intense, due to the contribution of the form factor of the Pt particles, but also broader, due to the orientation distribution of the lattice. The above difference may therefore result from the defference in the distortion of the long-range order of the micromain structure: the distortion in our case is smaller than that in their case. The large distortion of the lattice makes the lattice factor a constant value independent of q at $q > q_{m2}$, so that the scattering depends only on the local spatial arrangement of the particles within the cylinders at $q > q_{m2}$. Thus, their scattering curves that show a very broad peak should reflect the particle−particle spacing as they asserted. The large excess scattering arising from the metal particles formed in the microdomains was discerned in our systems also at $q > 0.25$ nm^{-1} (see Figures 3 and 5). However, in our systems we could not clearly discern the broad peak due to the particle−particle spacing.

Judging from our results in Figures 3 and 5 for the system composed of the Pd particles in the lamellar system, it is puzzling to note that their SAXS results, *L*, for Pd(Cp^N)PA-*block*-MTD having lamellar microdomains showed only very small change in the SAXS profiles before and after the reduction: the large excess scattering due to the Pd particles was not observed even after the reduction. Probably we may need more information about the results in order to clearly understand the results.

5. Conclusion

Growth of Pd nanoparticles after T-jump of concentrated PI-*b*-P2VP block copolymer and P2VP homopolymer solution in benzyl alcohol and $Pd(acac)_2$ was observed by the time-resolved SAXS. The SAXS profiles measured were composed of the following two contributions: the scattering from the microdomain structure formed by block copolymers in the solution and that from the Pd nanoparticles created via the reduction process of Pd(II) ions after T-jump. The microdomain structures formed before reduction were slightly changed during the reduction process as described in section 4.4. By analyzing the scattering from the Pd nanoparticles with eqs 3 and 6, we could evaluate time evolution of mean radius, reduced standard deviation of radius, and total volume of Pd nanoparticles in the concentrated PI-*b*-P2VP and P2VP solutions after T-jump. These results and the information obtained in our previous communication,[18] as schematically demonstrated in Figure 1, conclude that the formation of Pd nanoparticles after T-jump of PI-*b*-P2VP solution proceeds as follows: Pd(II) ions existing uniformly in space are reduced into Pd(0) atoms; Pd(0) atoms associate into Pd nanoparticles after an induction period, followed by a selective incorporation in P2VP lamellar microdomains due to selective interactions with P2VP block chains; the growth of Pd nanoparticles stops because an increased number of sites adsorbed by P2VP chains effectively hinder translational freedom of the nanoparticles in the polymer matrix. The final size and total volume of Pd nanoparticles created depend on the reduction temperature, but the NG mechanism of Pd nanoparticles itself does not change by the reduction temperature. The growth kinetics of Pd nanoparticles in a P2VP homopolymer solution is different from that in a PI-*b*-P2VP block copolymer solution with a microdomain structure, implying that the NG mechanism may depend on the space confinement of P2VP chains. We found that time-resolved SAXS measurement is very useful technique for in-situ observation of metal nanoparticle formation.

Although the real-space analysis via TEM observation is also very helpful, the samples used in this experiment (the concentrated solution in benzyl alcohol) could not easily allow the real-space analysis, unfortunately. This work should be deserved for future investigations. The TEM studies after evaporation of the solvent indicated that the Pd nanoparticles are selectively incorporated in P2VP lamellar microdomains and that the lamellae conserve long-range order, as reported elsewhere.[17,18,31]

References and Notes

(1) Toshima, N.; Takahashi, T. *Bull. Chem. Soc. Jpn.* **1992**, *65*, 400.
(2) Brust, M.; Walker, M.; Bethell, D.; Schiffrin, D. J.; Whyman, R. *J. Chem Soc., Chem. Commun.* **1994**, 801.
(3) Pileni, M. P. *Langmuir* **1997**, *13*, 3266.
(4) Antonietti, M.; Förster, S.; Hartmann, J.; Oestreich, S. *Macromolecules* **1996**, *29*, 3800.
(5) Seregina, M. V.; Bronstein, L. M.; Platonova, O. A.; Chernyshov, D. M.; Valetsky, P. M. *Chem. Mater.* **1997**, *9*, 923.
(6) Underhill, R. S.; Liu, G. *Chem. Mater.* **2000**, *12*, 3633.
(7) Spatz, L. P.; Mössmer, S; Hartmann, C.; Möller, M. *Langmuir* **2000**, *16*, 407.
(8) Ng Cheong Chan, Y.; Schrock, R. R.; Cohen, R. E. *Chem. Mater.* **1992**, *4*, 24.

(9) Ng Cheong Chan, Y.; Craig, G. S. W.; Schrock, R. R.; Cohen, R. E. *Chem. Mater.* **1992**, *4*, 885.
(10) Sohn, B. H.; Cohen, R. E. *Acta Polym.* **1996**, *47*, 340.
(11) Ciebien, J. F.; Cohen, R. E.; Duran, A. *Supermol. Sci.* **1998**, *5*, 31.
(12) Saito, R.; Okamura, S.; Ishizu, K. *Polymer* **1992**, *33*, 1099.
(13) Saito, R.; Okumura, S.; Ishizu, K. *Polymer* **1993**, *34*, 1183, 1189.
(14) Spatz, J. P; Roescher, A.; Möller, M. *Adv. Mater.* **1996**, *8*, 337.
(15) Fogg, D. E.; Radzilowski, L. H.; Blanski, R.; Schrock, R. R.; Thomas, E. L. *Macromolecules* **1997**, *30*, 417.
(16) Zehner, R. W.; Sita, L. R. *Langmuir* **1999**, *15*, 6139.
(17) Tsutsumi, K.; Funaki, Y.; Hirokawa, Y.; Hashimoto, T. *Langmuir* **1999**, *15*, 5200.
(18) Hashimoto, T.; Harada, M.; Sakamoto, N. *Macromolecules* **1999**, *32*, 6867.
(19) Horiuchi, S.; Sarwar, M. I.; Nakao, Y. *Adv. Mater.* **2000**, *12*, 1507.
(20) Horiuch, S.; Fujita, T.; Hayakawa, T.; Nakao, Y. *Langmuir* **2003**, *19*, 2973.
(21) Sakamoto, N.; Hashimoto, T. *Macromolecules* **1998**, *31*, 3292.
(22) Pontoni, D.; Narayanan, T.; Rennie, A. *Langmuir* **2002**, *18*, 56.
(23) Hashimoto, T.; Tsutsumi, K.; Funaki, Y. *Langmuir* **1997**, *13*, 6869 and references therein.
(24) Tsutsumi, K.; Funaki, Y.; Hirokawa, Y.; Hashimoto, T. *Langmuir* **1999**, *15*, 5200.
(25) Hashimoto, T.; Suehiro, S.; Shibayama, M.; Saijo, K.; Kawai, H. *Polym. J.* **1981**, *13*, 501. Fujimura, M.; Hashimoto, T.; Kawai, H. *Mem. Fac. Eng., Kyoto Univ.* **1981**, *43*, 224. Suehiro, S.; Saijo, K.; Ohta, Y.; Hashimoto, T.; Kawai, H. *Anal. Chim. Acta* **1986**, *189*, 41.
(26) Guinier, A.; Fournet, G. *Small-Angle Scattering of X-rays*; Wiley: New York, 1955.
(27) Hashimoto, T.; Sakamoto, N., manuscript in preparation.
(28) Kerker, M. *Scattering of Light and Other Electromagnetic Radiation*; Academic Press: New York, 1969.
(29) Okumura, A.; Tsutsumi, K.; Hashimoto, T. *Polym. J.* **2000**, *32*, 520.
(30) Hashimoto, T.; Okumura, A.; Tanabe, D. *Macromolecules* **2003**, *36*, 7324.
(31) Hashimoto, T.; Hasegawa, H. *Trans. Mater. Res. Soc. Jpn.* **2004**, *29*, 77.
(32) Kinning, D. J.; Thomas, E. L. *Macromolecules* **1984**, *17*, 1712.
(33) Percus, J. K.; Yevick, G. J. *Phys. Rev.* **1958**, *110*, 1.
(34) Avrami, M. J. *J. Chem. Phys.* **1939**, *7*, 1103.

MA051233J